Desorption Kinetics and Activation Energy for Cobalt Octaethylporphyrin from Graphite at the Phenyloctane Solution-Graphite Interface: An STM Study

Ashish Bhattarai, Ursula Mazur, and K W Hipps*

Department of Chemistry, Washington State University, Pullman, WA 99164-4630

Abstract

Temperature dependent desorption rates and desorption energies are determined from a monolayer assembly at the solution solid interface. Scanning tunneling microscopy (STM) was used to measure molecular scale temperature dependent desorption of cobalt(II) octaethylporphyrin (CoOEP) at the phenyloctane solution - highly ordered pyrolytic graphite (HOPG) interface. At lower temperatures, monolayer formation of metal(II) octaethylporphyrin (MOEP) on HOPG from solution was found to be completely controlled by kinetics and the adlayer formed was stable up to 70 °C. Significant desorption of CoOEP from the HOPG surface was observed above 80 °C on a time scale of hours. CoOEP desorbs from HOPG into phenyloctane at a rate of 0.0055 ± 0.0007 min^{-1} at 90 °C, 0.013 ± 0.001 min^{-1} at 100 °C, and 0.033 ± 0.003 min^{-1} at 110 °C. From these temperature and time dependent measurements, assuming an Arrhenius rate law, the activation energy of molecular desorption at the solution-solid (SS) interface was determined using studies solely based on STM. The desorption energy

of CoOEP from HOPG into phenyloctane is determined to be $1.05 \times 10^2 \pm 0.028 \times 10^2$ kJ/mol. NiOEP desorption occurs at a slower rate and is homogeneous across HOPG terraces, unlike the inhomogeneous desorption observed on Au(111). A previous study performed on Au(111), reported that the rate of desorption of CoOEP is 0.004 min^{-1} at 135 °C. The calculated desorption rate on HOPG in this work is 0.22 min^{-1}, making the rate of desorption of CoOEP from HOPG three orders of magnitude greater than from Au(111). On the other hand, for solution concentrations of the order of 120 μM, a dense monolayer is formed within seconds. For this fast adsorption process, where a full monolayer coverage occurs, the surface coverage of MOEP on both surfaces was determined by the relative concentration of each species in the phenyloctane solution. The rates of adsorption (for concentrations near 100 μM) are found to be within 20% of each other. The surface structures of both the NiOEP and CoOEP on HOPG and Au(111) are identical and can be described by A = 1.30 ± 0.02 nm, B = 1.40 ± 0.02 nm, and α = 57° ± 1° with an area of 1.82 ± 0.04 nm^2/molecule, giving similar adsorbate-adsorbate interactions.

Introduction

The study of organic self-assembled molecules (SAMs) supported on an atomically flat surface has attracted an enormous amount of attention. Rightly so, due to its actual and potential applications in modern technology, molecular electronics,[1,2] spintronics,[3] solar cells,[4,5] catalysis[6], sensors[7,8,9] and various other areas. Study of these SAMs at the solution-solid (SS) compared to vacuum-solid interface has a special prominence since it can be conducted under conditions where bi-directional exchange between the surface and surrounding medium is possible and equilibrium might be established. Unlike the vacuum-solid interface, at the SS interface solvent molecules play a critical role. In addition to the adsorbate-substrate interactions, one must consider solvent-solvent, solvent-adsorbate, and solvent-substrate interactions. These interactions are complex; but in the special case where equilibrium is established, important parameters can sometimes be estimated using various computational and experimental techniques.[10-12] Of the very few instruments capable of investigating the SS boundary at the molecular scale, scanning tunneling microscopy (STM) is especially appropriate. STM has the ability to resolve structures on a molecular and even sub-molecular scale. It can perform these studies in various solution environments, at varying temperature, pressures, and concentrations, and on various surfaces. These studies allow a direct single molecule level probe of surface structure, adsorption and reaction kinetics, and even molecular movies of the evolution of equilibrium. This last capability can provide experimental values for critical functions of state.

While UHV studies allow for improved understanding of adsorbate-substrate interactions and of surface localized transformations, they are extremely limited for studying systems driven by thermodynamic and/or kinetic processes where molecular exchange occurs on and off the

surface. When a SS pair is present, these phase exchange processes can be addressed. Although the SS pair provides a foundation for studying these adsorption-desorption processes, it is often difficult to distinguish between those that are thermodynamically driven, kinetically driven, or where both processes are active. A few early studies of long chain substitute alkanes on graphite indicated that exchange between solution and surface could be fast on the order of seconds. [13,14] Intuitively, one may think of temperature dependent studies to identify and separate these processes.[12] Hence, there has been a recent dramatic increase in temperature dependent STM studies at the SS interface. [12 2122] Outside of temperature dependent studies, there have been only a few successful attempts to separate kinetically driven from thermodynamically controlled processes at the SS interface. It was shown that the addition of a species different than the one at the surface can yield both thermodynamic and kinetic products.[23] Similarly, concentration [12,24] dependent and two component [25- 29] studies can also yield useful information about driving forces. Unfortunately, not all surface structures are stable and accessible at higher temperatures, allowing only a small temperature range for studying these processes. Hence, very little quantitative information regarding the thermodynamics and kinetics at the SS boundary is known.[30] Furthermore, most of the quantitative analysis found in the literature deals with phase transition processes.[30]

Very few SS interface STM studies deal with the actual adsorption strength of molecules on surfaces. One such study is the adsorption/desorption kinetics of cobalt(II)octaethylporphyrin (CoOEP) at phenyloctane-Au(111) interface.[31] It was shown that the CoOEP desorbs extremely slowly from the Au(111) surface and the rate of desorption was determined to be 0.004 min^{-1} at 135 °C. This showcased how strongly porphyrins can adsorb on a surface even though no covalent or ionic bonds are involved. While there have been a handful of adsorption studies of

metal porphyrins on highly ordered pyrolytic graphite (HOPG) in the past, these studies at most qualitatively suggested that the surface structures observed near room temperature were kinetically controlled. The study by Bhattarai et al[31] was the first to provide an imaging based quantitative measure of the desorption rate at the SS interface for any substrate.

It is well known that the substrate can play an important role in the assembly of organic molecules. Self-Assembly of an adlayer can be heavily influenced either by the electronic coupling between the adsorbate and substrate or by the arrangement/packing of atoms in the underlying substrate. For example, under ultra-high vacuum (UHV) conditions, coronene adsorbed on Ag(111),[32] has a slightly different lattice constant compared to coronene on HOPG,[33] and MoS_2.[33] This difference was attributed to tilting of coronene molecules with respect to the underlying HOPG and MoS_2 layers. More recently, it was shown that coronene on Ge(001) adsorbs in an upright configuration, contrary to the previously mentioned studies.[34] The authors argued that while the electron density on the metal surface enhances the adsorbate-substrate interactions, the semiconducting behavior of Ge(001) allows for the π-π interactions between the adsorbates to outweigh the adsorbate-substrate interactions. Another such surface induced interaction is of vanadyl phthalocyanine (VOPc) adsorbed on Si(111)-(7x7) and on Ag(111).[35] It was shown that VOPc adsorbs with oxygen-up configuration on Ag(111) whereas, on Si(111) it prefers oxygen-down configuration. Although the underlying surface can play a strong role in monolayer formation, these interactions are poorly explored. A deeper knowledge and understanding of the assembly of organic molecules on various surfaces is required.

In this work we will go far beyond the study reported by Bhattarai and coworkers.[31] We will make desorption rate measurements at different temperatures in order to extract the energy of activation for the desorption process – the first such determination for any system by STM at

the SS interface. We also will explore the effects of changing the substrate from Au(111) to HOPG. This will allow a quantitative evaluation of the relative desorption kinetics associated with changing only the substrate.

NiOEP will be used as a tracer for desorbed CoOEP from the HOPG surface. It is well known that cobalt and nickel porphyrins or phthalocyanines at the solution-solid and vacuum-solid interface can be well distinguished in an STM image.[31,36-38] Thus, the loss of a CoOEP from the surface and the subsequent replacement by NiOEP can be separately distinguished and easily measured. Using this tracer methodology, we will demonstrate that monolayer formation at temperatures close to room temperature is very fast and dominated by kinetics. We will demonstrate that the rate of desorption of CoOEP at the phenyloctane-HOPG interface is almost non-existent at room temperatures and is very slow even at temperatures up to 70 °C. Whereas, at 90, 100, and 110 °C desorption occurs on a time scale of hours. By comparing these measured desorption rates to those determined for CoOEP desorption from the phenyloctane-Au(111) interface,[31] valuable quantitative insights into the role of the substrate at the SS interface will be provided.

Experimental Section

The experimental procedures used in this work are similar to those in Bhattarai et al.[31] There are, however a number of differences such as temperatures studied, solution concentration determinations, and substrates used. Moreover, for the metal octaethylporphyrin (MOEP)/HOPG system, unlike the MOEP/Au system, tip induced changes must be considered.

CoOEP, 2,3,7,8,12,13,17,18-Octaethyl-21H,23H-porphine cobalt(II), and 2,3,7,8,12,13,17,18-Octaethyl-21H,23H-porphine nickel(II) [NiOEP] were purchased from

Aldrich and Frontier Scientific respectively. The structure of a metal(II) octaethylporphyrin (MOEP) can be seen in Figure 1. Phenyloctane (98%) was purchased from Aldrich and was subjected to further purification as described in reference 31. HOPG of grade-I and II were purchased from SPI Supplies and were freshly cleaved using scotch tape before the sample was deposited.

UV Visible spectroscopy on saturated and filtered solutions of porphyrins in phenyloctane was used to determine solubility at room temperature. The measured solubility of CoOEP in phenyloctane was 3.9×10^{-4} M or 0.23 g/L and that of NiOEP was 5.4×10^{-4} M or 0.32 g/L. The highest concentration solutions used in these experiments was 1.5×10^{-4} M and most were less than 1.1×10^{-4} M. Thus, all solutions were below the solubility limit.

STM images were recorded using a Molecular Imaging (now Agilent) Pico 5 STM equipped with a scanner capable of imaging a maximum area of 1 $\mu m^2$and having an overall current sensitivity of 1 nA/V. The Agilent environmental chamber was used for all experiments and argon atmosphere was maintained. STM tips were primarily prepared by cutting and sometimes electrochemically etching the $Pt_{0.8}Ir_{0.2}$ wire purchased from California Fine Wire Company. An exception to this occurred while examining tip effects (described in the supplemental materials) in which case both etched and cut tips were used equally. Images were typically obtained in constant current mode at a sample potential of +0.5 to +0.7 V and a tunneling current of 20 to 50 pA. Images of sizes ranging from 30 x 30 nm^2 to 50 x 50 nm^2 were collected at a scan rate of 4.7 lines/sec, giving a total image time of just under 2 min. Images larger than 50 x 50 nm^2 were scanned at a slower scan rate of 3.3 to 3.9 lines/sec, giving a total image time of roughly 2.5 min. The temperature of the sample was controlled by a variable-temperature hot stage using a Lakeshore 330 auto-tuning temperature controller. The environmental chamber was purged with

99.996% Ar (A-L Compressed Gases, Inc., Spokane, WA) at all times. Before imaging, samples were allowed to sit for 30 minutes to one hour inside the environmental chamber purged with Ar at 2.5 standard cubic feet per hour (scfh). During imaging, Ar was continuously purged at 0.5 scfh into the environmental chamber.

Solutions of CoOEP and NiOEP were prepared by dissolving solid porphyrin compounds in phenyloctane. Concentrations were measured using a UV-visible spectrophotometer where the extinction coefficient of each species had been previously measured by applying Beer's law to a series of dilutions of a known concentration solutions. Stock solutions of 1.1×10^{-4} M CoOEP and 1.5×10^{-4} M NiOEP were prepared separately. A custom made solution cell STM sample holder was used to accommodate large volumes (up to 100 μL) of solution in contact with the HOPG surface.

During the sample heating process, the temperature of the sample was ramped at a rate of 5 °C per minute, allowing the sample to reach the desired temperature (within the 90 - 110 °C range) in 20 min. The sample then was held at the desired final temperature for the desired time period. After this fixed time heating, samples were rapidly cooled to room temperature by turning the heater off. Samples were then allowed to equilibrate for at least 60 minutes prior to recording any images. All STM images were background subtracted using SPIP image processing software.

Tip induced desorption of porphyrins is known in the literature, [36,39] and we noted occasional tip induced local changes in our samples. These events were dealt with by moving to new areas to continue measurement. The role of tip induced defects in this study is discussed in the Supplemental Section.

Results and Discussion

Figure 1 presents separate STM images of CoOEP (110 μM in phenyloctane) and of NiOEP (150 μM in phenyloctane) at the solution-HOPG interface at 25 °C under Ar. As reported in the literature, the center of CoOEP appears bright and the center of NiOEP appears dark.[31,37,40] The cross-sectional profile of CoOEP in Figure 1 clearly shows a peak at the center of the molecule, whereas for NiOEP a depression is seen which gives rise to its dark appearance. It must be noted that the localization of the peak or depression is dependent on the tip sharpness and bias voltage. Hence, CoOEP sometimes appears as a wider bright region. In all cases where various tips are used, CoOEP always appears brighter, hence taller than the NiOEP at the voltages used in this study when both species are in the same image. We must proceed with caution while imaging CoOEP at the solution-HOPG interface, since it is well known to bind atmospheric O_2 at room temperatures.[20] This changes the appearance of oxygen bound CoOEP molecules (O_2-CoOEP appear dark) under STM and can be misinterpreted as NiOEP. Hence, prior to recording all STM images, Ar was flowed at 2.5 scfh for at least 15 minutes before deposition and 0.5 scfh at all times to ensure ambient air was replaced by Ar. Thus, any possibility of oxygen binding to CoOEP and oxidation of Co^{+2} ion was unlikely.

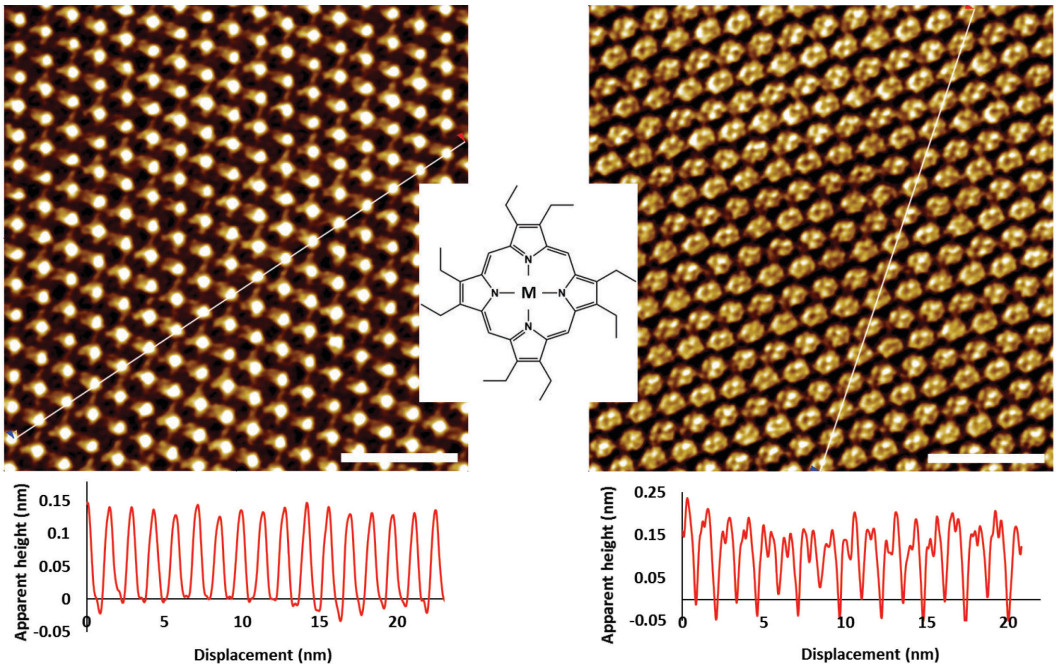

Figure 1. Constant current STM images of MOEP at the phenyloctane-HOPG interface. An image of CoOEP is shown on the left and of NiOEP on the right side in the Figure. The bottom portion of the Figure shows the cross-sectional apparent height of each of the MOEP. STM images were obtained under set point conditions of +0.7 V bias and 50 pA tunneling current. Scale bar is 5 nm.

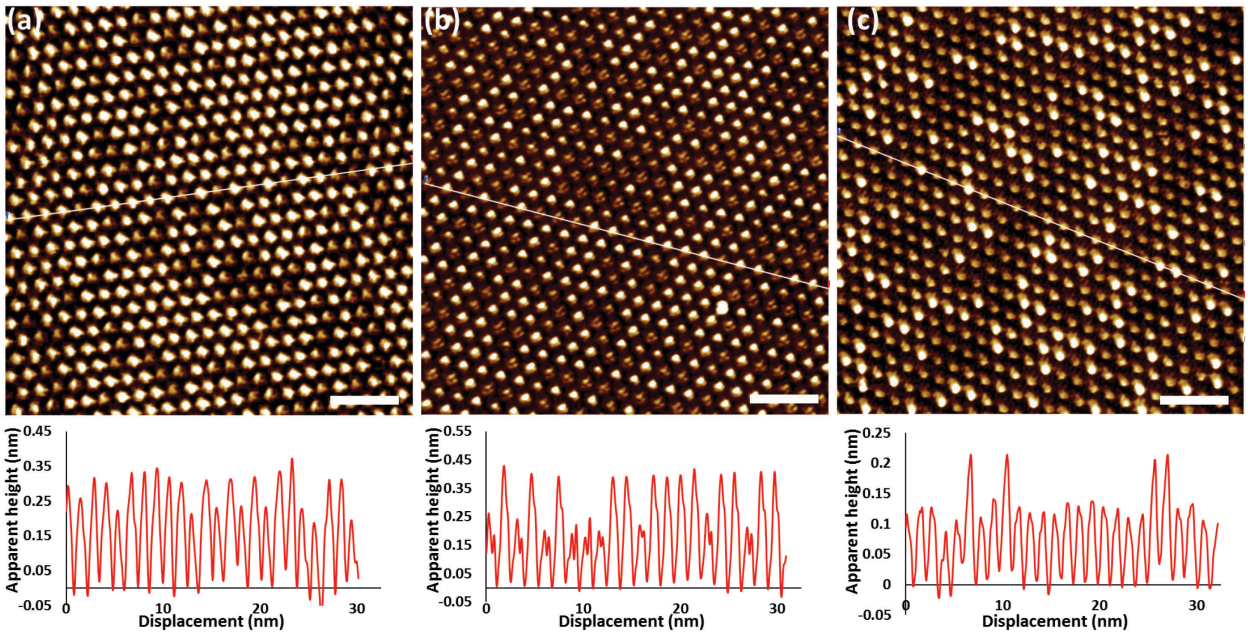

Figure 2. Constant current STM images of mixtures of CoOEP and NiOEP in varying ratios at the solution-HOPG interface of (a) $X_{NiOEP} = 0.28 \pm 0.03$, and $\Theta_{NiOEP} = 0.25 \pm 0.02$; (b) $X_{NiOEP} = 0.55 \pm 0.03$, and $\Theta_{NiOEP} = 0.53 \pm 0.02$; (c) $X_{NiOEP} = 0.76 \pm 0.03$, and $\Theta_{NiOEP} = 0.76 \pm 0.02$. Set point conditions were +0.5 V bias and 50 pA tunneling current. Scale bar is 5 nm.

When a mixture of CoOEP and NiOEP solutions of varying relative concentrations are deposited on HOPG, a mixed monolayer is formed consisting of bright (CoOEP) and dark (NiOEP) species as depicted in Figure 2. It can be seen in Figure 2 that the surface coverage of bright species decreases as the relative concentration of CoOEP in solution decreases. Similarly, the surface coverage of dark species increases as the relative concentration of NiOEP in solution is increased. In order to report surface concentrations, we define Θ_{NiOEP} as the number of NiOEP molecules in a given area divided by the total number of molecules in the same given area on HOPG. This notation works here because of the monolayer coverage observed in all images. For solution concentrations, we define X_{NiOEP} as the number of moles of NiOEP divided by the total number of moles of porphyrins in solution. Thus, it is a mole fraction of total porphyrins

present, not of total moles present (solvent is excluded). Using this notation, four different mixtures of CoOEP and NiOEP were prepared, allowed to equilibrate on HOPG, and the resulting surface layers (still in contact with the solution) were then studied under STM. In order to ensure statistical significance, numerous (more than 10 per mixture) STM images of all the mixtures were analyzed. From these numerous images, an average value of Θ_{NiOEP} was obtained for each value of X_{NiOEP}. Using these data, an adsorption isotherm can be created and it is plotted for data acquired at 25 °C in Figure 3. From this room temperature isotherm, it can be seen that Θ_{NiOEP} and X_{NiOEP} are essentially equal.

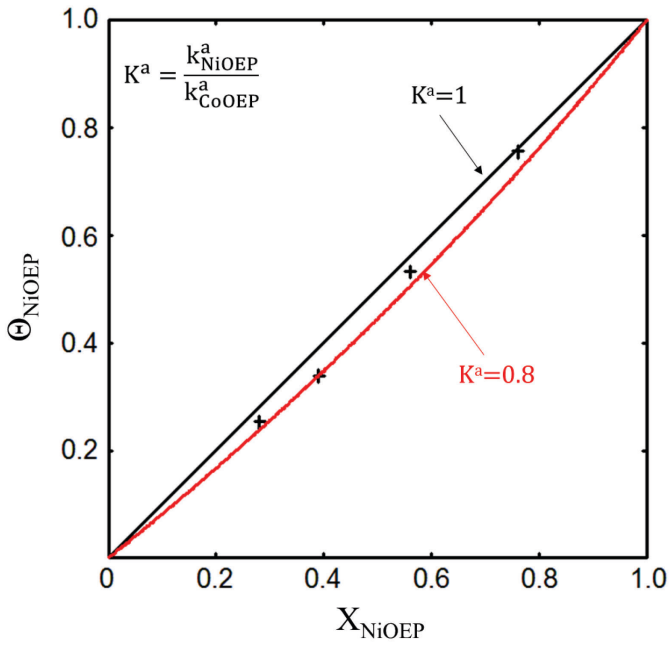

Figure 3. Adsorption isotherm at 25 °C: Surface coverage of NiOEP relative to CoOEP on HOPG (Θ_{NiOEP}) versus fractional concentration of NiOEP in phenyloctane solution (X_{NiOEP}).

In-situ imaging experiments were performed for various mixtures where the sample was heated at different temperatures. Figure 4 is a representation of the in-situ images taken at 25, 50, and 70 °C for $X_{NiOEP} = 0.38 \pm 0.04$. Averaged over all images acquired over the duration of six to ten hours at each temperature, $\Theta_{NiOEP} = 0.34 \pm 0.03$ at 25 °C, $\Theta_{NiOEP} = 0.34 \pm 0.02$ at 50 °C, and $\Theta_{NiOEP} = 0.33 \pm 0.02$ at 70 °C. Investigation of sequential images separated by a few minutes apart at various temperatures up to 60 °C shows an even more important feature. There is no sign of molecules exchanging between the surface and solution, clearly indicating that the rate of desorption is extremely slow even at elevated temperatures. That is, no bright site is seen to change to dark, or vice versa. Thus, the relative coverage was independent of temperature over the 25 to 70 °C range. Our only indication of in-situ molecular exchange was seen at 70 °C and is depicted in Figure 5. The red hexagon and oval shapes in Figure 5 are drawn as markers. With respect to these markers, only one site changes its appearance from image (b) to image (c). A dark site (circled white) is converted into a bright site, meaning that a NiOEP molecule on the surface is desorbed and the vacancy that is left behind is filled by a CoOEP molecule. It must be noted that no other sequential images obtained within a period of up to 15 min at 70 °C show any sign of molecular adsorption/desorption processes. Thus, even at 70 °C the rate of desorption of CoOEP and NiOEP is very slow. This parallels the behavior of CoOEP and NiOEP adsorbed from phenyloctane on Au(111).[31] In order to record any quantitative desorption at 70 °C, we would have to monitor the same area on the surface on a time scale of hours.

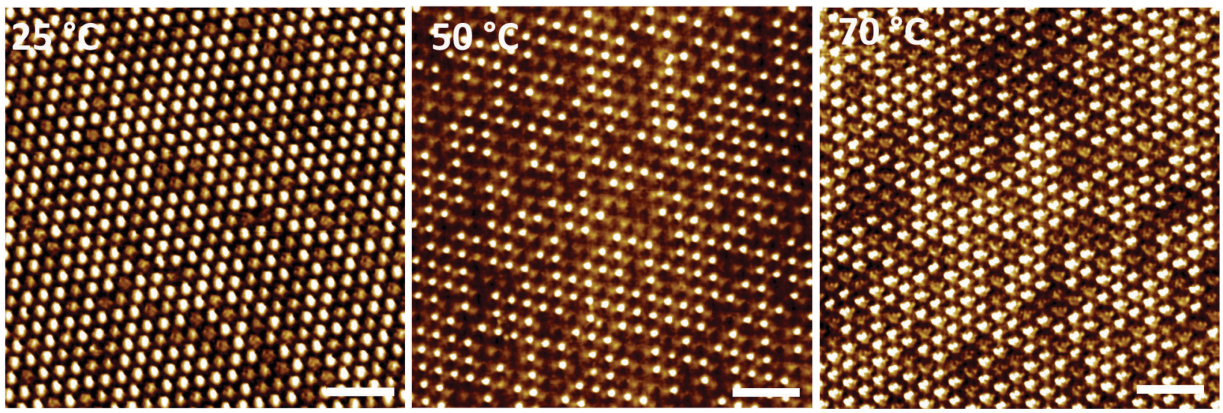

Figure 4. *In-situ* temperature dependent STM images of monolayers formed from $X_{NiOEP} = 0.38$ where $\Theta_{NiOEP} = 0.34 \pm 0.03$ on HOPG at 25, 50, and 70 °C different temperatures. Set point condition was +0.5 V bias and 50 pA tunneling current. Scale bar is 5 nm.

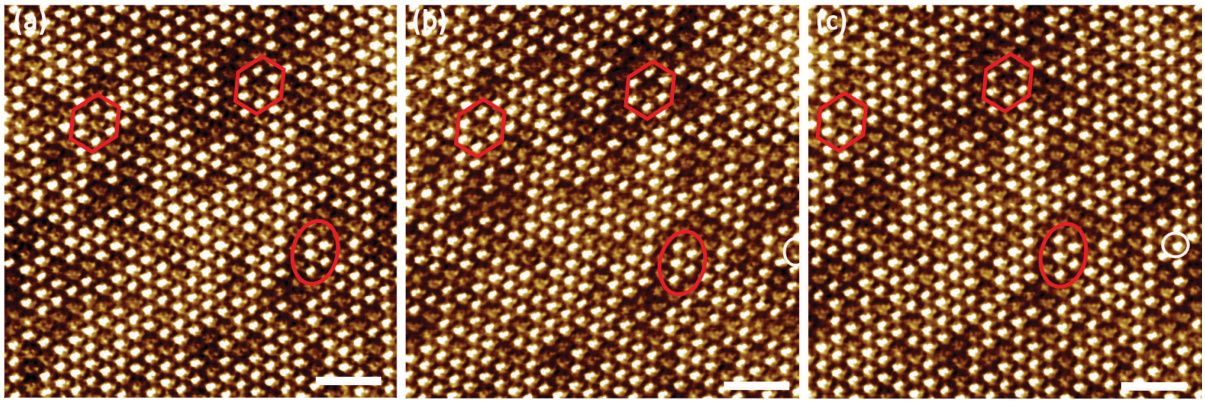

Figure 5. Sequential STM images of $X_{NiOEP} = 0.38$ at 70 °C. Each image is separated by 108 sec apart. Set point condition was +0.7 V bias and 50 pA tunneling current. Scale bar is 5 nm.

Knowing that the rate of desorption near 300 K is extremely slow, and that the monolayer forms in a matter of seconds, it is clear that the isothermal adsorption data displayed in Figure 3 resulted entirely from a kinetically controlled process. There is no equilibrium between solution and surface. Thus, the data in Figure 3 may be understood through an analysis given in reference

31. Because the rate of formation of a monolayer is many orders of magnitude faster than the rate of desorption, Θ_{NiOEP} or Θ_N (for brevity) at steady state is given by,

$$\theta_N = (1 - e^{-\bar{k}Mt})\left(\frac{k_N^a X_N}{\bar{k}}\right) \qquad \text{(eqn. 1)}$$

and, $\bar{k} = \left(k_N^a X_N + k_C^a X_C\right) = k_N^a X_N + k_C^a (1 - X_N)$ (eqn. 2)

where, k_N^a and k_C^a are the rate constants for the adsorption of NiOEP and CoOEP, respectively. X_N and X_C are the mole fractions of NiOEP and CoOEP (relative to total porphyrin) in solution, respectively. M is the total molarity of porphyrins in the solution. At lower temperatures where the desorption rate is extremely slow or non-existent, $\theta_N = \left(\frac{k_N^a X_N}{\bar{k}}\right)$. Thus, Θ_N depends only on the mole fraction and relative rates of adsorption of CoOEP and NiOEP. This relationship is represented in Figure 3 by the smooth curves. The black curve is for the case where $k_N^a = k_C^a$, and the red curve is for the case where $k_N^a = 0.8k_C^a$. Thus, the rates of adsorption of CoOEP and NiOEP are within 20 % of each other and are probably the same.

A complete kinetic analysis of the monolayer formation requires accounting for monolayer nucleation and growth and for reorganization of molecules along the domain boundaries. Studying the domain sizes on both HOPG and Au(111) could provide valuable qualitative insights into the adsorption mechanisms of these MOEP molecules. Very rarely we found domain boundaries of MOEP on HOPG, whereas there were plentiful on Au(111). This suggests that all of the above mentioned processes may be different on the two substrates. Quantitative evaluation of these parameters is beyond the scope of present study. Instead, we focus on measuring an effective relative overall rate for monolayer formation. We can state that

the relative rates of monolayer formation of CoOEP and NiOEP [on both HOPG and Au(111)] are similar.

We now turn attention to the desorption process. Based on our experience with MOEP on Au(111),[31] we expected that with increasing temperature the rate of desorption from HOPG will become significant and measureable. However, the in situ experiments reported above become less effective at higher temperatures. In cases where steady state will only occur in a time of the order of an hour or longer, a different method is used -- the procedure reported in reference 31. First, a dense monolayer of one of the MOEP (CoOEP) on HOPG was prepared. Then, an excess of the species not present in the monolayer (NiOEP) was added such that the solution in contact with the surface has a mixture of both MOEP species. Because of the excess amount of the second species in the solution, if any desorption of the first species occurs then the second species is more likely to fill the vacant site on the surface and can be easily detected in an STM image due to the difference in molecular contrast. The sample is then heated to higher temperatures (>70 °C), held at that temperature for a certain time period, and then rapidly cooled to room temperature to perform STM imaging. Because of the fast adsorption and slow desorption below 80 °C of either MOEP, this ex-situ technique captures the results of the adsorption-desorption processes that occur at higher temperatures.

To show that this method correctly reflects the very low desorption rates seen near room temperature, a confirming experiment was performed. STM images were obtained at 25 °C of a monolayer of CoOEP prior to and following being covered for 24 hours with a solution having X_N = 0.80. These images (Figure 6) clearly show that at low temperatures no exchange is occurring even on a time scale of many hours. Obvious exchanges can be observed only above 80 °C after 30 min of heating. In related experiments at 25 °C, the surface was first exposed to a

pure solution of one MOEP and then a mixed solution was added within a few seconds. In both cases, only the first MOEP was ever observed in the monolayer. Thus, monolayer formation on HOPG (as in the case of Au(111)) is very fast and forms within a few seconds.

At temperatures above 70 °C the stability of the initial monolayer is lost. At 90, 100, and 110 °C, significant changes in the monolayer were seen. Thus, these three temperatures were used to determine the rates of desorption and subsequently the activation energy for desorption of CoOEP from HOPG at the phenyloctane-HOPG interface. Here, focus will be placed on CoOEP desorption from HOPG in order to compare it to the known value on Au(111). It is worth noting that NiOEP followed a similar trend to that observed for CoOEP and that its desorption is uniform on the HOPG surface. This surface uniformity of desorption of NiOEP on HOPG is quite different than the case of NiOEP desorption from Au(111).[31] As demonstrated by Bhattarai and coworkers, [31] NiOEP preferentially desorbs from step edges and reconstruction lines. No such position dependent desorption was observed on HOPG.

Monolayer samples of CoOEP were deposited from pure CoOEP in phenyloctane solutions and imaged by STM. Then, a large excess of a solution of NiOEP and CoOEP (X_N = 0.80) was added. This sample was then heated to 90, 100, or 110 °C for time intervals of 30 min each up to 3 h in total. After each time interval, the sample was cooled quickly to room temperature and multiple measurements of 6 to 15 different areas of 50 x 50 nm^2 sized areas (one image has roughly 2000 total molecules) were taken to ensure statistical significance. Figure 7 shows STM images of a sample (initially covered by a monolayer of CoOEP at the phenyloctane solution-HOPG interface) after 30 min exposure to a solution of X_N = 0.80 at 90, 100, and 110 °C. It is clear that as the temperature is increased, more CoOEP is desorbed and is replaced by NiOEP.

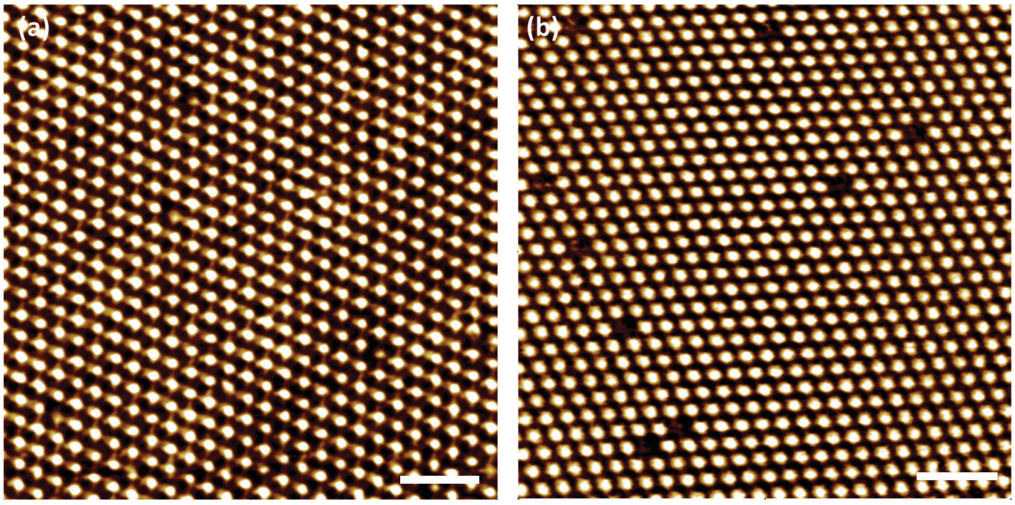

Figure 6. STM images obtained at 25 °C. (a) Solution of CoOEP in phenyloctane on HOPG; (b) monolayer from (a) following a 24 hour exposure to a solution having $X_N = 0.80$. Scale bar is 5 nm.

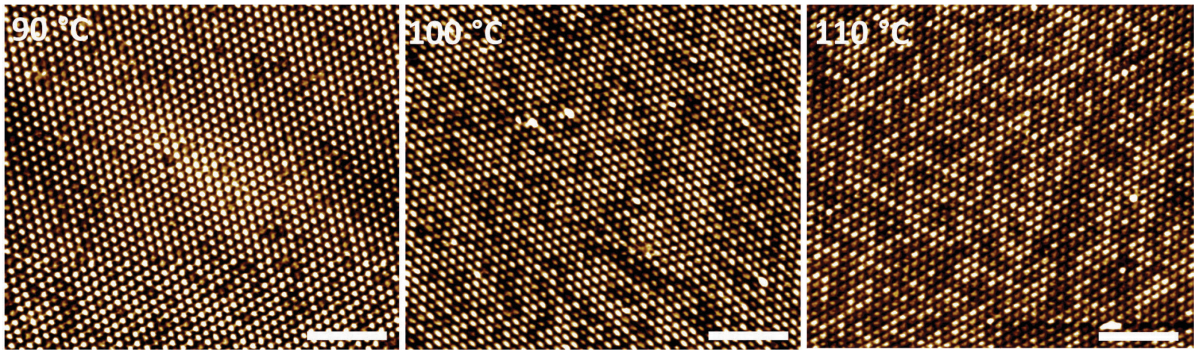

Figure 7. 50 x 50 nm^2 STM images of a surface initially covered by a monolayer of CoOEP on HOPG following 30 min exposure to a solution of $X_N = 0.80$ at 90 °C (left), 100 °C (middle), and 110 °C (right). Set point conditions were +0.7 V bias and 50 pA tunneling current. Scale bar is 10 nm.

Values of Θ_N obtained by repeated annealing of samples in 30 min intervals for a total of up to 3 h at 90, 100, and 110 °C are given in Figure 8. What is obvious from the raw data is that the rate of desorption is still slow even at 110 °C, with hours of heating time required for the

surface composition to reach steady state. It is also a bit surprising at first that at the highest temperature the steady state surface concentration of NiOEP is greater than X_N. On reflection, this result is expected if the rate of desorption of CoOEP is greater than for NiOEP at 110 °C. In order to extract quantitative desorption rates and energies, the model used for CoOEP desorption from Au(111) was used. In this model, the rate of appearance of NiOEP on a complete monolayer covered by both NiOEP and CoOEP is equal to: (the rate of disappearance of CoOEP × the probability that this vacant site will be filled by NiOEP) – (the rate of disappearance of NiOEP × the probability that this vacant site will be replace by CoOEP). For the case of fast adsorption where we assume $k_N^a = k_C^a$, and slow desorption, Θ_N after an annealing time, t, is given by,

$$\Theta_N(t) = (\frac{1}{b})(1 - e^{-bk_C^d X_N t}) = \frac{k_C^d X_N}{k_C^d X_N + k_N^d (1 - X_N)}\left[1 - e^{-bX_N k_c^d t}\right] \qquad \text{(eqn. 3)}$$

and, $$b = \left\{1 + \left[(1 - X_N)\left(\frac{k_N^d}{k_C^d X_N}\right)\right]\right\} \qquad \text{(eqn. 4)}$$

The most direct approach to determining the parameters in this expression is to fit the complete set of Θ_N(t,T) data to equation 3. However, since the k_i^d are temperature dependent, this gives six parameters that must be determined. Our data set is too small to give reliable values for so many parameters. Thus, some simplification is required in order provide a useful analysis. We approached the problem in two different ways. The critical parameters of desorption energy and k_c^d that result are essentially independent of method.

In the first method, use is made of the Arrhenius model for the temperature dependence of the rate constants, $k_i^d = k_i^0 e^{\frac{-\Delta E_i}{RT}}$, where 'i' represents either 'C' for CoOEP or 'N' for NiOEP,

and ΔE_i is the desorption energy of species i. It is also useful to define the ratio $K^d = \frac{k_N^d}{k_C^d} = K^0 e^{(\Delta E_C - \Delta E_N)/RT}$, where $K^0 = \frac{k_N^0}{k_C^0}$. Using these definitions and assumptions, equation 3 can be rewritten as follows:

$$\Theta_N(t) = \frac{1}{\left[1+\left\{\left(\frac{1-X_N}{X_N}\right)K^0 e^{\frac{\Delta E_C - \Delta E_N}{RT}}\right\}\right]}\left[1 - \exp\left\{\left[-X_N k_C^0 e^{\frac{-\Delta E_C}{RT}}\right]\left[\left(K^0 e^{\left(\frac{\Delta E_C - \Delta E_N}{RT}\right)}\left(\frac{1-X_N}{X_N}\right)\right)+1\right]t\right\}\right] \quad \text{(eqn. 5)}$$

This reduces the number of parameters from six to four. It is found, however, that least squares fitting yield results where the uncertainties in several of the parameters exceed their values. Thus a further reduction in the number of parameters is required. Given the similar nature in size, weight, and solubility of CoOEP and NiOEP and similar ionic radii of Co^{+2} and Ni^{+2} one would expect the vibrational motion of the entire molecule normal to the HOPG surface would be similar for both species. Interpreting the k_i^0 to be an attempt frequencies and relating it to this vibrational frequency leads one to conclude that k_i^0 should be very similar of both porphyrins and therefore $K^0 \approx 1$.

Fixing $K^0 = 1$, we used non-linear least squares to optimize equation 5 to the Θ_N(t,T) data taking ΔE_C, ΔE_N, and k_C^0 as adjustable parameters. The result of this optimization is given as the smooth curves in Figure 8(a). Optimized values of ΔE_C, ΔE_N, and k_C^0 were found to be 1.05 x 10^2 ± 0.03 x 10^2 kJ/mol, 1.05 x 10^2 ± 0.03 x 10^2 kJ/mol, and 6.2 x 10^{12} ± 5.6 x 10^{12} min^{-1} respectively. Using these optimized values, rates of desorption for CoOEP from HOPG are estimated. For CoOEP, average k_C^d's are found to be 0.0048, 0.012, and 0.030 min^{-1} at 90, 100, and 110 °C respectively. Obtaining $\Theta_N^{t\to\infty}$ values at all temperatures would allow for a more robust determination of the k_N^d values, but there are experimental problems that make this difficult to do accurately. With our current experimental design, long annealing times lead to

solvent evaporation and eventually to CoOEP and/or NiOEP becoming saturated and precipitating out of solution. In order to avoid this complication, we restricted measurement times to where the solution concentration remained well under the saturation concentration. Clearly, however, the uncertainty in k_i^0 (as determined by this method) are still very large and we should refrain from conclusive statements regarding their values.

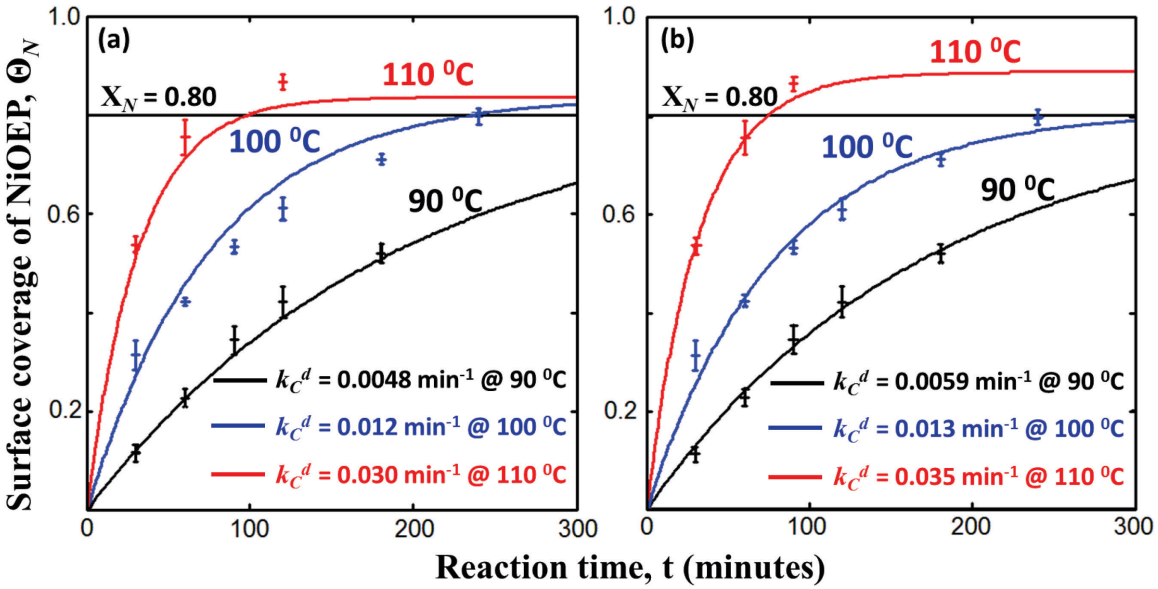

Figure 8. Best fit curves for surface coverage of NiOEP, Θ_{NiOEP} with reaction time and average k_C^d's at 90 °C (black curve), 100 °C (blue curve), and 110 °C (red curve) for: (a) K^0 = 1 and optimized values of ΔE_C, ΔE_N, and k_C^0 for the entire time (t/min) and temperature (T/°C) data set; (b) optimized values of k_C^0 and K^d at each T.

In order to determine more precise values of k_C^d and to support the validity of the desorption energies, a second analysis method was used. In method 2, one fits the curves given in equation 3 (and 4) for varying k_C^d and K^d values independently at each temperature. k_C^d and K^d values were optimized using a non-linear least square fit to produce a best fit curve at each temperature. These optimized curves are presented in figure 8(b). At 90 °C, k_C^d = 0.0059 ±

0.0002 min^{-1} and K^d = 0.91 ± 0.3; at 100 °C, $k_C{}^d$ = 0.013 ± 0.0004 min^{-1} and K^d = 0.94 ± 0.1; at 110 °C, $k_C{}^d$ = 0.035 ± 0.0002 min^{-1} and K^d = 0.49 ± 0.01. These values of the $k_C{}^d$ are in excellent agreement with those determined by method 1. The K^d values at 90, and 100 °C are close to 1 (0.9) and are the same within one standard deviations. The K^d value at 110 °C is roughly 0.5. Due to the likely differences in the temperature dependence of rate constants for CoOEP and NiOEP, it is possible for the K^d value at 110 °C to be smaller than ones obtained at lower temperatures. Furthermore, K^d = 0.49 ± 0.010 at 110 °C indicates that the CoOEP desorbs from HOPG faster than NiOEP which is also in agreement with the experimental data.

Using the rate values obtained by method 2 at 90, 100, and 110 °C, a plot of $ln(k_C^d)$ versus 1/T gives a straight line (Figure 9). Assuming an Arrhenius type activated process (as we did above) the slope of this plot gives $-\Delta E_d/R$. Thus, the energy for desorption of CoOEP is calculated to be 1.03 x 10^2 ± 0.40 kJ/mol and the attempt frequency is found to be 3.7 x 10^{12} ± 3.9 x 10^{12} min^{-1}. These values are quite similar to those obtained from the first method. In both methods, $k_C{}^d$ values can be described as 0.0055 ± 0.0007 min^{-1} at 90 °C, 0.013 ± 0.001 min^{-1}at 100 °C, and 0.033 ± 0.003 min^{-1} at 110 °C and ΔE_C is given by 1.05 x 10^2 ± 0.03 x 10^2 kJ/mol. In order to obtain values of $k_N{}^d$ and ΔE_N with equal precision, similar desorption experiments with NiOEP as a starting monolayer on HOPG would be of great value and these are underway.

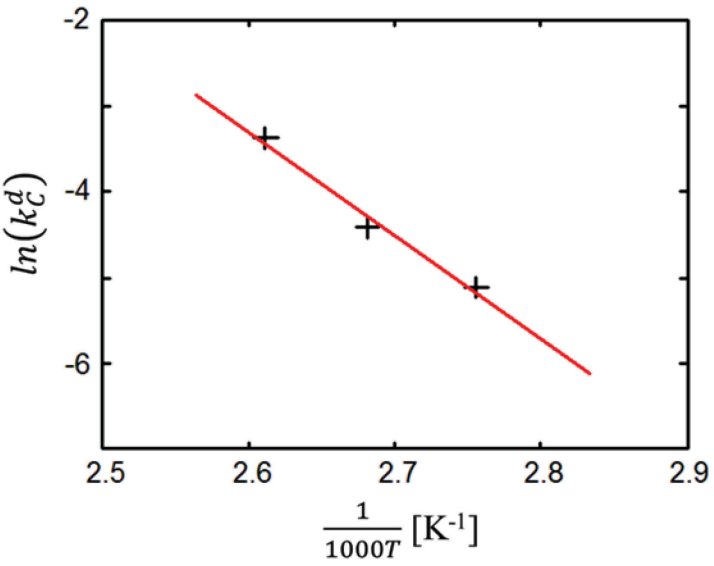

Figure 9. Plot of ln(k) versus 1/T.

It is useful to consider why the individual two-parameter fits recreate the surface coverage versus time plots so much better than the three parameter fit of the entire data set. The simplest explanation is that the three parameter fit (method 1) forces the ratio of the pre-exponentials to be fixed and independent of temperature. Neither may be the case. A different way of interpreting the rate equation is by using the Eyring equation wherein the entropic and enthalpic contributions to formation of the activated state are considered. In this model, k_i^0 is replaced by $\frac{kT}{h} e^{\frac{\Delta S^+}{R}}$. Thus there may be both explicit and implicit temperature dependences in the k_i^0.

Using the values for ΔE_C and k_C^d consistent with both methods described earlier, one predicts an average desorption rate of 0.22 min^{-1} for CoOEP from HOPG in phenyloctane at 135 °C. This is 55 times greater than the observed desorption rate for CoOEP in the same solvent but desorbing from Au(111) at 135 °C.[31] This dramatic change in desorption rate with varying substrate in the absence of covalent interactions demonstrates the critical role the substrate can

play in determining the composition and stability of an adlayer at the solution-solid interface. The choice of substrate can easily cause a particular solvent-solute pair to yield an adlayer that is entirely kinetically controlled, thermodynamically controlled, or slowly evolving with time.

We also report on the molecular spacing for the pure CoOEP and NiOEP monolayers at the phenyloctane solution-HOPG interface. For CoOEP, A = 1.27 ± 0.02 nm, B = 1.40 ± 0.02 nm, and α = 57° ± 1°; for NiOEP, A = 1.28 ± 0.02 nm, B = 1.39 ± 0.02 nm, and α = 57° ± 1°. Under UHV conditions, the eight ethyl groups of NiOEP vapor deposited on Au(111) were resolved.[41] These data showed that there are 2 molecules per unit cell on Au in UHV, where the unique molecules were slightly rotated with respect to one another. In this work, we were not able to resolve the ethyl groups and hence we chose a unit cell consisting of only one molecule. Given the precision of our measured spacing, both the CoOEP and NiOEP can be described as having a unit cell dimensions of A = 1.28 ± 0.02 nm, B = 1.40 ± 0.02 nm, and α = 57° ± 1° with an area of 1.79 ± 0.04 nm^2/molecule on HOPG. On Au(111),[31] both NiOEP and CoOEP occupy 1.87 ± 0.04 nm^2/molecule. Based on the similarity of the packing on the two substrates, it is likely that MOEP have similar adsorbate-adsorbate interactions on HOPG and on Au(111). Also, with similar solubility (3.9 x 10^{-4} and 5.4 x 10^{-4} M for CoOEP and NiOEP respectively), they are likely to have similar adsorbate-solvent interactions. Hence, the difference in adsorption strength of CoOEP on HOPG and Au(111) may arise almost entirely from differences in adsorbate-substrate interactions. If one attributes the difference in desorption rates from HOPG and from Au at 135 °C as entirely due to differences in desorption energy, one predicts that the desorption energy from Au(111) into phenyloctane should be roughly 1.19 x 10^2 kJ/mole.

Conclusions

For the first time a complete quantitative analysis of the kinetics of molecular desorption at the solution-solid interface has been performed using scanning tunneling microscopy. The surface dependence of the adsorption/desorption kinetics at the solution solid interface has been analyzed. At temperatures near 20 °C, monolayer coverage of MOEP both at phenyloctane solution-HOPG and phenyloctane solution-Au(111) interfaces is completely controlled by kinetics. In both cases, a dense monolayer of MOEP forms within seconds, whereas desorption is extremely slow even above 70 °C. For a mixture of CoOEP and NiOEP in phenyloctane, the overall rates of adsorption (to form a complete monolayer) on either Au(111) or HOPG are nearly species independent and proportional to the relative concentration of each species in solution. On the other hand, significant MOEP desorption into phenyloctane on a scale of hours occurs only above 80 °C from HOPG and 130 °C from Au(111). The rate of desorption of CoOEP from HOPG is two orders in magnitude larger than from Au(111) at 135 °C. Due to the similar areas occupied by NiOEP and CoOEP on both surfaces, and similar solubility in phenyloctane, the difference in adsorption strength is likely due to the difference in MOEP-HOPG and MOEP-Au(111) interactions. Another distinguishing feature of the substrate dependence of desorption is that it is site specific for NiOEP on Au(111) but uniform desorption is observed from HOPG terraces.

CoOEP desorbs twice as fast as NiOEP at the phenyloctane-HOPG interface at 110 °C. Given the similar nature in size and solubility of CoOEP and NiOEP and similar ionic radii of Co^{+2} and Ni^{+2}, these differences most likely arise from differences in Ni-HOPG and Co-HOPG interactions. The desorption rates reported here are for molecules desorbing from a full

monolayer. Desorption rates from grain boundaries and defects, or from small islands of molecules may differ.

ASSOCIATED CONTENT

Supporting Information. Analysis of tip induced desorption. This material is available free of charge via the Internet at http://pubs.acs.org.

Acknowledgement

The US National Science foundation generously provided support for this work in the forms of grants CHE-1403989 and CHE-1112156.

REFERENCES

[1] Wang, L.; Chen, Q.; Pan, G.; Wan, L.; Zhang, S.; Zhan, X.; Northrop, B. H.; Stang, P. J. Nanopatterning of Donor/Acceptor Hybrid Supramolecular Architectures on Highly Oriented Pyrolytic Graphite: A Scanning Tunneling Microscopy Study. *J. Am. Chem. Soc.* **2008**, *130*, 13433-13441.

[2] Samori, P.; Yin, X.; Tchebotareva, N.; Wang, Z.; Pakula, T.; Jackel, F.; Watson, M. D.; Venturini, A.; Mullen, K.; Rabe, J. P. Self-Assembly of Electron Donor-Acceptor Dyads into Ordered Architectures in Two and Three Dimensions: Surface Patterning and Columnar "Double Cables". *J. Am. Chem. Soc.* **2004**, *126*, 3567-3575.

[3] Kim, H.; Chang, Y. H.; Lee, S.; Kim, Y.; Kahng, S. Switching and Sensing Spin States of Co-Porphyrin in Bimolecular Reactions on Au(111) Using Scanning Tunneling Microscopy. *ACS Nano* **2013**, *7*, 9312-9317.

[4] Wang, Q.; Campbell, W. M.; Bonfantani, E. E.; Jolley, K. W.; Officer, D. L.; Walsh, P. J.; Gordon, K.; Humphry-Baker, R.; Nazeeruddin, M. K.; Gratzel, M. Efficient Light Harvesting by Using Green Zn-Porphyrin-Sensitized Nanocrystalline TiO2 Films. *J. Phys. Chem. B* **2005**, *109*, 15397-15409.

[5] Campbell, W. M.; Jolley, K. W.; Wagner, P.; Wagner, K.; Walsh, P. J.; Gordon, K. C.; Schmidt Mende, L.; Nazeeruddin, M. K.; Wang, Q.; Gratzel, M.; Officer, D. L. Highly Efficient Porphyrin Sensitizers for Dye-Sensitized Solar Cells. *J. Phys. Chem. C* **2007**, *111*, 11760-11762.

[6] Bourikas, K.; Kordulis, C.; Lycourghiotis, A. The Role of the Liquid-Solid Interface in the Preparation of Supported Catalysts. *Catalysis Reviews – Science and Engineering* **2006**, *48*, 363-444.

[7] Yoshimoto, S.; Suto, K.; Itaya, K.; Kobayashi, N. Host-guest recognition of calcium by crownether substituted phthalocyanine array on Au(111): relationship between crown moieties and gold lattice. *Chem. Commun.* **2003**, 2174-2175.

[8] Piot, L.; Silly, F.; Tortech, L.; Nicolar, Y.; Blanchard, P.; Roncali, J.; Fichou, D. Long-Range Alignments of Single Fullerenes by Site-Selective Inclusion into a Double-Cavity 2D Open Network. *J. Am. Chem. Soc.* **2009**, *131*, 12864-12865.

[9] Flechtner, K.; Kretschmann, A.; Steinruck, H.; Gottfried, J. M. NO-Induced Reversible Switching of the Electronic Interaction between a Porphyrin-Coordinated Cobalt Ion and a Silver Surface. *J. Am. Chem. Soc.* **2007**, *129*, 12110-12111.

[10] Song, W.; Martsinovich, N.; Heckl, W. M.; Lackinger, M. Born-Haber Cycle for Monolayer Self-Assembly at the Liquid-Solid Interface: Assessing the Enthalpic Driving Force. *J. Am. Chem. Soc.* **2013**, *135*, 14854-14862.

[11] MacCloud, J. M.; Chaouch, Z. B.; Perepichka, D. F.; Rosei, F. Two-Dimensional Self-Assembly of a Symmetry-Reduced Tricarboxylic Acid. Langmuir **2013**, *29*, 7318-7324.

[12] Blunt, M. O.; Adisoejoso, J.; Tahara, K.; Katayama, K.; Van der Auweraer, M.; Tobe, Y.; De Feyter, S. Temperature-Induced Structural Phase Transitions in a Two-Dimensional Self-Assembled Network. *J. Am. Chem. Soc.* **2013**, *135*, 12068-12075.

[13] F. Stevens, F.; Beebe, T. P. Jr. Dynamical Exchange Behavior in Organic Monolayers Studied by STM Analysis of Labeled Mixtures. *Langmuir* **1999**, 15, 6884-6889.

[14] Padowitz, D. F.; Sada, D. M.; Kemer, E. L.; Dougan, M. L.; Xue, W. A.; Molecular Tracer Dynamics in Crystalline Organic Films at the Solid-Liquid Interface. *J. Phys. Chem. B* **2002**, 106, 593-598.

[15] Gutzler, R.; Sirtl, T.; Dienstmaier, J. F.; Mahata, K.; Heckl, W. M.; Schmittel, M.; Lackinger, M. Reversible Phase Transition in Self-Assembled Monolayers at the Liquid-Solid Interface: Temperature-Controlled Opening and Closing of Nanopores. *J. Am. Chem. Soc.* **2010**, *132*, 5084-5090.

[16] Marie, C.; Silly, F.; Tortech, L.; Mullen, K.; Fichou, D. Tuning the Packing Density of 2D Supramolecular Self-Assemblies at the Solid-Liquid Interface Using Variable Temperature. *ACS Nano* **2010**, *4*, 1288-1292.

[17] Gutzler, R.; Cardenas, L.; Rosei, F. Kinetics and thermodynamics in surface-confined molecular self-assembly. *Chemical Sciences* **2011**, ***2*,** 2290-2300.

[18] Kim, K.; Plass, K. E.; Matzger, A. J. Structure of and Competitive Adsorption in Alkyl Dicarbamate Two-Dimensional Crystals. *J. Amer. Chem. Soc.* **2005**, *127*, 4879-4887.

[19] Jahanbekam, A.; Vorpahl, S.; Mazur, U.; Hipps, K. W. Temperature Stability of Three Commensurate Surface Structures of Coronene Adsorbed on Au(111) from Heptanoic Acid in the 0 to 60 0C Range. *J. Phys. Chem. C* **2013**, *117*, 2914-2919.

[20] Friesen, B. A.; Bhattarai, A.; Mazur, U.; Hipps, K. W. Single Molecule Imaging of Oxygenation of Cobalt Octaethylporphyrin at the Solution/Solid Interface: Thermodynamics from Microscopy. *J. Am. Chem. Soc.* **2012**, *134*, 14897-14904.

[21] English, W. A.; Hipps, K. W. Stability of a Surface Adlayer at Elevated Temperature: Coronene and Heptanoic Acid on Au(111). *J. Phys. Chem. C* **2008**, *112*, 2026-2031.

[22] Yang, Yan; Zimmt, Matthew B. Shape Amphiphiles in 2-D: Assembly of 1-D Stripes and Control of Their Surface Density. *J. Phys. Chem. B.* **2015***, DOI:* 10.1021/acs.jpcb.5b00291.

[23] Ahn S.; Matzger, A. J. Additive Perturbed Molecular Assembly in Two-Dimensional Crystals: Differentiating Kinetic and Thermodynamic Pathways. *J. Am. Chem. Soc.* **2012**, *134*, 3208-3214.

[24] Bellec, A.; Arrigoni, C.; Schull, G.; Douillard, L.; Fiorini-Debuisschert, C.; Mathevet, F.; Kreher, D.; Attias, A.; Charra, F. Solution-growth kinetics and thermodynamics of nanoporous self-assembled molecular monolayers. *The Journal of Chemical Physics* **2011**, *134*, 124702.

[25] Coenen, M. J. J.; Cremers, M.; den Boer, D.; van den Bruele, F. J.; Khoury, T.; Sintic, M.; Crossley, M. J.; van Enckevort, W. J. P.; Hendriksen, B. L. M.; Elemans, J. A. A. W.; Speller, S. Little exchange at the liquid/solid interface: defect-mediated equilibration of physisorbed porphyrin monolayers. *Chem. Commun.* **2011**, *47*, 9666-9668.

[26] Coenen, M. J. J.; Khoury, T.; Crossley, M. J.; Hendriksen, B. L. M.; Elemans, J. A. A. W.; Speller, S. Nanostructuring of self-assembled porphyrin networks at a solid/liquid interface: local manipulation under global control. *ChemPhysChem* **2014**, *15*, 3484-3488.

[27] Ikeda, T.; Asakawa, M.; Goto, M.; Miyake, K.; Ishida, T.; Shimizu, T. STM Observation of Alkyl-Chain-Assisted Self-Assembled Monolayers of Pyridine-Coordinated Porphyrin Rhodium Chlorides. *Langmuir* **2004**, *20*, 5454-5459.

[28] Otsuki, J.; Kawaguchi, S.; Yamakawa, T.; Asakawa, M.; Miyake, K. Arrays of Double-Decker Porphyrins on Highly Oriented Pyrolytic Graphite. *Langmuir* **2006**, *22*, 5708-5715.

[29] Ikeda, T.; Asakawa, M.; Miyake, K.; Goto, M.; Shimizu, T. Scanning Tunneling Microscopy Observation of Self-Assembled Monolayers of Strapped Porphyrins. *Langmuir* **2008**, *24*, 12877-12882.

[30] Mazur, U.; Hipps, K. W. Kinetic and Thermodynamic Processes of Organic Species at the Solution Solid Interface: The view through an STM. *ChemComm* **2015** DOI: 10.1039/c4cc09840d.

[31] Bhattarai, A.; Mazur, U.; Hipps, K. W. A Single Molecule Level Study of the Temperature Dependent Kinetics for the Formation of Metal Porphyrin Monolayers on Au(111) from Solution. *J. Am. Chem. Soc.* **2014**, *136*, 2142-2148.

[32] Lackinger, M.; Griessl, S.; Heckl, W. M.; Hietschold, M. Coronene on Ag(111) Investigated by LEED and STM in UHV. *J. Phys. Chem. B.* **2002**, *106*, 4482-4485.

[33] Walzer, K.; Sternberg, M.; Hietschold, M. Formation and characterization of coronene monolayers on HOPG(0001) and MoS2: a combined STM/STS and tight-binding study. *Surface Science* **1998**, *415*, 376-384.

[34] Martínez-Blanco, J.; Mascaraque, A.; Dedkov, Y. S.; Horn, K. Ge(001) As a Template for Long-Range Assembly of π-Stacked Coronene Rows. *Langmuir* **2012**, *28*, 3840-3844.

[35] Eguchi, K.; Takagi, Y.; Nakagawa, T.; Yokoyoma, T. Molecular Orientation and Electronic States of Vanadyl Phthalocyanine on Si(111) and Ag(111) Surfaces. *J. Phys. Chem. C* **2013**, *117*, 22843-22851.

[36] Hipps, K. W.; Scudiero, L.; Barlow, D. E.; Cooke, M. P. Jr. A Self-Organized 2-Dimensional Bifunctional Structure Formed by Supramolecular Design. *J. Am. Chem. Soc.* **2002**, *124*, 2126-2127.

[37] Barlow, D. E.; Scudiero, L.; Hipps, K. W. Scanning Tunneling Microscopy Study of the Structure and Orbital-Mediated Tunneling Spectra of Cobalt(II) Phthalocyanine and Cobalt(II) Tetraphenylporphyrin on Au(111): Mixed Composition Films. *Langmuir* **2004**, *20*, 4413-4421.

[38] Scudiero, L.; Barlow, D. E.; Hipps, K. W. Physical Properties and Metal Ion Specific Scanning Tunneling Microscopy Images of Metal(II) Tetraphenylporphyrins Deposited from Vapor onto Gold(111). *J. Phys. Chem. B* **2000**, *104*, 11899-11905.

[39] Li, Min; den Boer, Duncan; Iavicoli, Patrizia; Adisoejoso, Jinne; Uji-I, Hiroshi; Van der Auweraer, Mark; Amabilino, David B.; Elemans, Johannes A.A.W.; De Feyter, Steven. Tip-Induced Chemical Manipulation of Metal Porphyrins at a Liquid-Solid Interface. *J. Am. Chem. Soc.* **2014**, *136*, 17418-17421.

[40] Scudiero, L.; Barlow, D. E.; Mazur, U.; Hipps, K. W. Scanning Tunneling Microscopy, Orbital-Mediated Tunneling Spectroscopy, and Ultraviolet Photoelectron Spectroscopy of Metal(II) Tetraphenylporphyrins Deposited from Vapor. *J. Am. Chem. Soc.* **2001** *123*, 4073-4080.

[41] Scudiero, L.; Barlow, D. E.; Hipps, K. W. Scanning Tunneling Microscopy, Orbital-Mediated Tunneling Spectroscopy, and Ultraviolet Photoelectron Spectroscopy of Nickel(II)Octaethylporphyrin Deposited from Vapor. *J. Phys. Chem. B* **2002**, *106*, 996-1003.